20th Australasian Fluid Mechanics Conference
Perth, Australia
5-8 December 2016

Simultaneous 2-Colour LIF & PIV Measurements of the Boundary Layer in a Differentially Heated Cavity

J. Yen, C. Lei and J. C. Patterson

School of Civil Engineering
The University of Sydney, New South Wales 2006, Australia

Abstract

Simultaneous planar temperature and velocity measurements using 2-colour/2-dye laser-induced fluorescence and particle image velocimetry of the natural convection flow in a differentially heated cubical cavity at the Rayleigh number of Ra = 3.1 $\times 10^8$ are reported for the first time. The results demonstrate the capability of such measurements to quantitatively capture the thermal and hydrodynamic boundary layers.

Introduction

Natural convection flows induced in cavities with differentially heated and cooled sidewalls is one of the classical heat and mass transfer problems. Furthermore, they are prototypical of many industrial processes, and their associated heat transfer is of significant practical importance, for example, in the thermal insulation of buildings [4] and cooling of (micro)electronics [8]. The evolution of this prototypical flow from an initially motionless and isothermal state with sudden isothermal or isoflux sidewall heating and cooling consists of: (a) formation of unsteady one-dimensional vertical boundary layers adjacent to the sidewalls, which exit into horizontal intrusions at the cavity ceiling and floor [6]; (b) passage of travelling waves from the leading-edge effect that transition the boundary layers to a steady two-dimensional state [1]; (c) secondary travelling waves in the vertical thermal boundary layers triggered by the arrival of the horizontal intrusions from the opposing sidewalls [6, 7]; and (d) slow transition to a steady state, or quasi-steady state for Rayleigh numbers larger than a critical value, with a thermally stratified core [7].

Computing the heat transfer rate in differentially heated cavities requires accurate measurement of the temperature field with high spatial resolution, as well as high temporal resolution for unsteady thermal flows, and so, despite its importance, has in the past been difficult with standard, intrusive thermocouples and thermistors. The more recently developed temperature measurement techniques of thermo-sensitive liquid crystals and molecular tagging offer desirable non-intrusive and whole-field measurements, but suffer from slow response times, small temperature ranges and poor spatial resolutions [2].

In contrast, laser-induced fluorescence (LIF), in which the fluorescence intensity of a dye is dependent on its temperature, can provide planar temperature measurements with higher spatial resolutions, large temperature ranges and high temperature sensitivities [2, 5]. Additionally, it can be extended to incorporate particle image velocimetry (PIV) for simultaneous velocity measurements.

This paper aims to demonstrate the capability of simultaneous 2-colour/2-dye LIF and PIV to quantitatively measure the thermal and hydrodynamic boundary layers adjacent to the cold sidewall of a differentially heated cavity. To this end, preliminary results of simultaneous planar temperature and velocity measurements using 2-colour/2-dye LIF and PIV are presented for the first time for the natural convection flow induced in a differentially heated cubical cavity following sudden differential heating and cooling from an initially motionless and isothermal state at the Rayleigh number of Ra = 3.1 $\times 10^8$.

Experimental Methods

Fluorescent Dyes & Tracer Particles

The principle of 2-colour/2-dye LIF is described by Sakakibara & Adrian [5], and is not repeated here for brevity. Rhodamine 610 Chloride (herein Rh-B) and Rhodamine 560 Chloride (herein Rh-110) were used as the temperature-dependent and -independent dyes, respectively, with concentrations of C_{Rh-B} = 0.125 mg/L and C_{Rh-110} = 5.50 mg/L in distilled water. Polyamid Seeding Particles (PSP) with a mean diameter of 20 μm were used as the PIV tracer particles with a concentration of C_{PSP} = 26.1 mg/L.

Experimental Setup

The experimental rectangular model was constructed from 10 mm thick perspex sheets and divided into three sections using two 2-mm thick copper plates, to form a middle cubical cavity of length H = 0.1 m and two water baths.

A laser beam produced by an Evergreen145 Nd:YAG laser with an excitation wavelength of λ_{ext} = 532 nm was expanded by a cylindrical lens with f = -10 mm focal length to form a laser light sheet and illuminate from below the mid-depth of the cubical cavity. The fluorescent light from the illuminated middle section was split by a beamsplitter into three LaVision ImagerSX 4M CCD cameras which had 2360 px $\times$ 1776 px resolution and 12-bit A/D dynamic range. The beamsplitter transmitted wavelengths greater than $\lambda > 570$ nm to the Rh-B camera and reflected the remainder to the Rh-110 camera. Additional bandpass filters with centre wavelengths of λ_{CW} = 600 nm, 550 nm and 532 nm and Full Width at Half Maximum values of 20 nm, 20 nm and 10 nm were, respectively, added to the Rh-B, Rh-110 and PIV cameras.

The field of view into the beamsplitter and cameras was aligned parallel to the cold sidewall of the cavity. Perspective calibration (image de-warping and alignment, and physical dimension mapping) was performed by taking images of a known grid pattern and least-squares fitting a 3rd-order polynomial function. The laser and cameras were operated at the same repetition and recording rate of F_s = 5 Hz.

Experimental Procedure

The experimental model was oriented such that the copper plates formed the vertical sidewalls of the cavity. Prior to starting the experiment, the temperature of the dye solution in the cavity was measured to be T_0 = 21.3°C, and water in two Julabo FP45-HE circulators was pre-cooled and -heated to T_C = 11.3°C and T_H = 31.3°C, respectively. The experiment commenced by pumping the cold and hot waters into the empty water bath sections of the experimental model, which filled up in

approximately ∼1 s. Images were recorded for 100 s using LaVision's Davis software, and the Prandtl and Rayleigh numbers were Pr = 6.78 and Ra = 3.1 $\times 10^8$, respectively.

Temperature Calibration

Temperature calibration was performed with the experimental model oriented such that the copper plates formed the horizontal ceiling and floor of the cavity. This allowed the cavity to be heated at 37°C from above and cooled to 9°C from below, producing a stable, thermally stratified field after 4.5 hours. The temperature calibration curve was obtained by least-squares fitting a 5th-order polynomial to the temperature-intensity ratio data, and had an average temperature sensitivity of -1.67%/K.

Post-Processing & Uncertainty Estimation

LIF image normalisation (to correct for vignetting effects and non-uniformities of the laser light sheet) and perspective correction were first performed using Davis. The normalisation was implemented according to:

$$I_{normalised}(x,y) = \frac{I_{original}(x,y)}{I_{ref}(x,y)} \frac{1}{N} \Sigma_i^N I_{ref}(x_i,y_i), \qquad (1)$$

where $I_{normalised}$ is the normalised image, $I_{original}$ the original image, I_{ref} the reference image, and N the number of image pixels. MATLAB was subsequently used to perform the ratiometric division (see [5]) and conversion to temperature. Then, each pixel was smoothed in time with a moving window of length 5, before a 11 px × 11 px moving average window was applied to each image.

PIV images were post-processed in Davis using an iterative multi-pass method with decreasing interrogation window size. The interrogation window was initially 64 px × 64 px with 50% overlap, and then decreased to 32 px × 32 px with 75% overlap for the second and third passes.

The total random temperature error was estimated from the undisturbed, isothermal region in the cavity core after start-up when the horizontal intrusions moved across the ceiling and floor. The uncertainty computed from twenty-one unprocessed temperature images was $2\sigma = \pm 1.4$ K with 95% confidence. This decreased to ±0.56 K after smoothing the images in time, and then to ±0.16 K after averaging in space.

Results and Discussion

Temperature & Velocity Field Development

The instantaneous temperature field at 15 s intervals from start-up is shown in figure 1, along with contour lines at 1 K intervals from T_0 = 21.3°C, and is overlaid with the velocity vector field. Here, x and y are the horizontal and vertical distances from the cavity centre, respectively. At t = 0 s, shown in figure 1a, the flow was essentially motionless and isothermal, albeit with an ambient cavity temperature slightly warmer than T_0. A warm thermal structure can also be observed in the top left corner of the cavity in figure 1a. This thermal structure was displaced as the flow developed and was replaced by a cool thermal structure that is visible from figure 1c to figure 1f. The persistence of this thermal structure indicated a systematic temperature bias that most likely originated in the system optics.

After commencing the experiment, by pumping the pre-cooled and -heated water into the empty water baths, the flow development displayed all the typical features of a natural convection flow in a differentially heated cavity that was described earlier. Initially, thin narrow boundary layers developed adjacent to the sidewalls. Figure 1b shows both the thermal and hydrodynamic boundary layers at t = 15 s which subsequently formed horizontal intrusions at the ceiling and floor. These intrusions moved across the cavity width, reaching the three-quarter mark at t = 30 s in figure 1c, and arrived at their opposing sidewall at approximately t ≈ 38 s. After this time, the cavity began a slow transition to a thermally stratified state. Additionally, the accumulation of cold and hot fluid near the bottom left and top right corners of the cavity, respectively, are clearly visible in figure 1e and figure 1f.

Boundary Layer Temperature & Velocity Profiles

Horizontal profiles of the non-dimensional temperature, H(η), and velocity, F′(η), as a function of Ostrach's [3] similarity parameter, η, near the cold sidewall at t = 30 s, when the boundary layer was steady but before the hot ceiling intrusion arrived, are shown in figure 2 for various heights, along with Ostrach's theoretical solutions for the present Prandtl number of Pr = 6.78.

Some of the non-dimensional temperature profiles, at y/H = 0.2 for example, had a large temperature value right next to the cold wall at η = 0, which was the result of the spatial averaging post-processing technique employed. This aside, the H(η) profiles collapsed well onto each other and displayed the same general shape as the theoretical profile. Additionally, the larger H(η) values beyond η > 2 quantitatively confirmed that the ambient cavity temperature measured by LIF was warmer than T_0.

On the other hand, the non-dimensional velocity profiles, while collapsing onto each other in the cavity interior, displayed large variations amongst themselves close to the wall between η = 0 and 2. Figure 2 also shows the F′(η) profiles were consistently smaller than the theoretical profile. These discrepancies could be due to the actual wall temperature being larger than the prescribed cold waterbath temperature of T_C = 11.3°C, which would reduce the temperature difference and hence natural convection flow velocity, as well as insufficient PSP tracer particles near the wall.

Local Nusselt Number & Wall Temperature Profiles

The temperature gradient along the cold sidewall was estimated by first finding, for each horizontal temperature profile, the local temperature minimum near the wall, and then least-squares fitting a line to the next four interior temperature data points. In this manner, any large temperature value right next to the cold wall, as observed in figure 2, was omitted from deleteriously affecting the result. The wall temperature, T_w, was subsequently estimated by extrapolating the fitted line to the wall.

Figure 3 shows the local Nusselt number, Nu, computed from the temperature gradient in red and T_w in blue along the cold sidewall at t = 60 s, as well as Nu from a laminar numerical simulation at t = 60 s in black, and T_C as the vertical blue line. The numerical simulation was identical to that reported in [9] but with a timestep of 0.01 s, without horizontal fins, and scaled to the height of H = 0.1 m.

The most prominent feature of the two profiles was their non-smooth variability along the wall. This was a result of the line fitting technique, in which a small change in temperature results in a large change in temperature gradient and, hence, extrapolated wall temperature. That being said, the experimental Nu profile varied around, and had the same general shape as, the numerical profile. However, the Nu near the top of the cavity above y/H > 0.4 was underestimated. This was most likely due to the inability of the cameras to capture and resolve the very thin boundary layer near the cold sidewall's leading-edge. Consequently, anomalous—even unrealistic at some heights—T_w values were produced above y/H > 0.35 compared to the

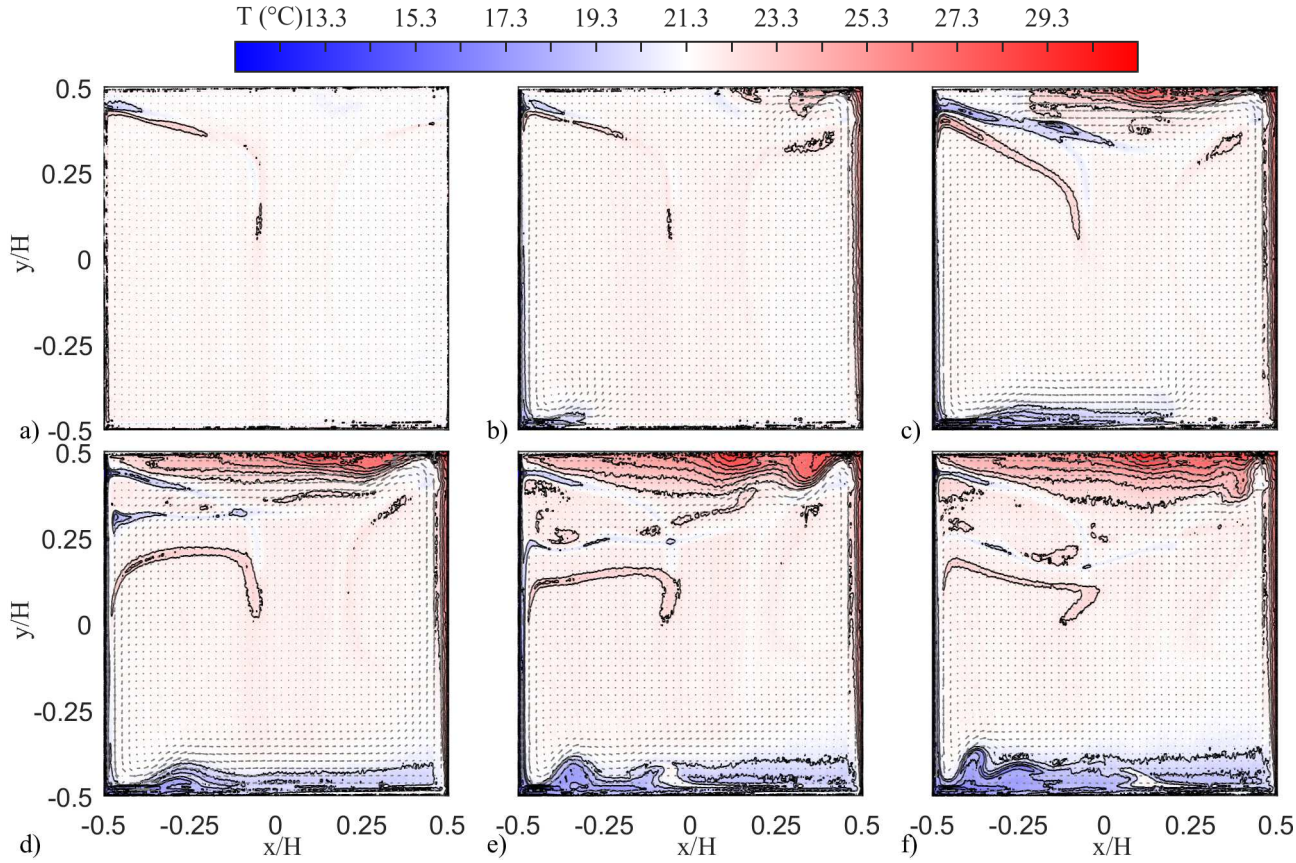

Figure 1: Temperature field overlaid with velocity vector field at a) t = 0 s; b) t = 15 s; c) t = 30 s; d) t = 45 s; e) t = 60 s; and f) t = 75 s. Temperature contour outlines are at 1 K intervals from T_0 = 21.3°C.

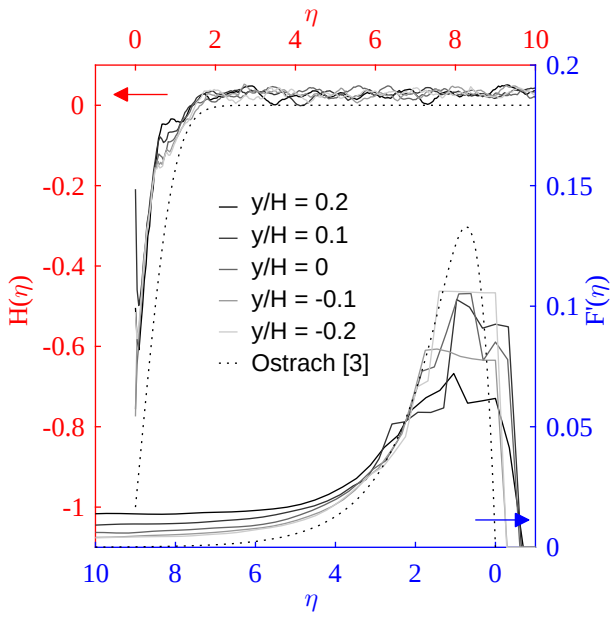

Figure 2: Non-dimensional temperature, H(η), and velocity, F′(η), profiles near the cold sidewall at various heights at t = 30 s, along with Ostrach's [3] solutions for Pr = 6.78.

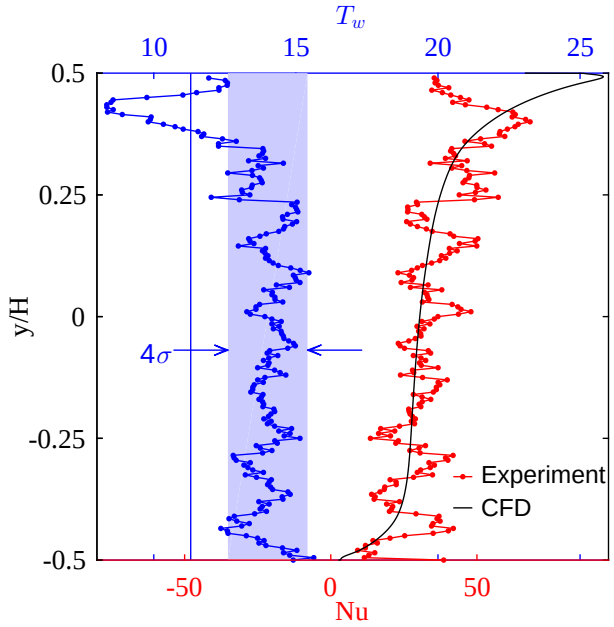

Figure 3: Local Nusselt number (red) and wall temperature (blue) profiles at t = 60 s. Local Nusselt number profile from CFD in black, and T_C = 11.3°C as the vertical blue line.

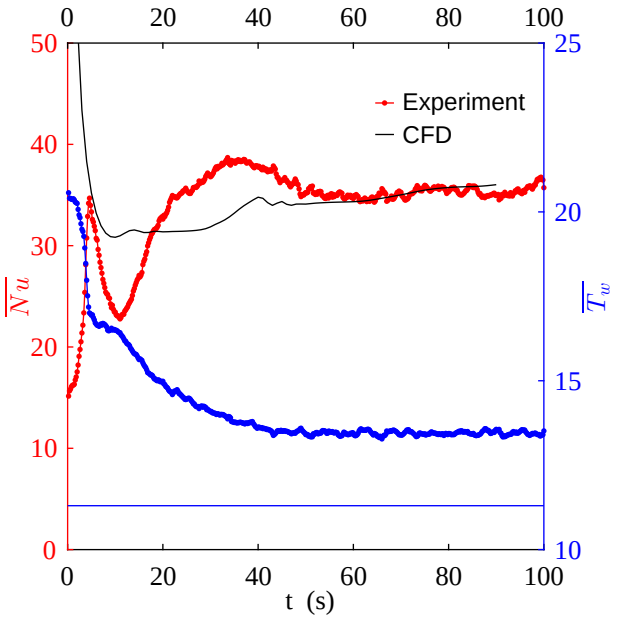

Figure 4: Time-series of wall-integrated Nusselt number (red) and wall-averaged temperature (blue). Wall-integrated Nusselt number from CFD in black, and T_C = 11.3°C as the horizontal blue line.

remainder of the profile which had an average value of 14°C. It should also be noted that the variation in T_w below y/H $<$ 0.35 was within the uncertainty of $2\sigma = \pm 1.4$ K.

Wall-Integrated Nusselt Number & Wall-Averaged Temperature

The wall-integrated Nusselt number, $\overline{Nu}$, and wall-averaged temperature, $\overline{T_w}$, are shown over time in figure 4, along with $\overline{Nu}$ from the numerical simulation and T_C as the black curve and horizontal blue line, respectively.

Unlike the numerical simulation, $\overline{Nu}$ rapidly increased after start-up until t = 4.6 s and then quickly decreased until 11 s. $\overline{Nu}$ subsequently displayed a more gradual change with time. The experimental and numerical $\overline{Nu}$ agreed well after the initial flow transients and arrival of the intrusions at the opposing sidewalls; t $>$ 50 s. This indicated that the underestimation of Nu near the top of the cavity at t = 60 s in figure 3 was cancelled by its overestimation in the remainder of the profile.

Similarly, $\overline{T_w}$ decreased rapidly after start-up, and then began to slow down after t $>$ 5 s, before obtaining a stable temperature of 13.4°C after t $>$ 43 s. While not shown for brevity, the temperature and velocity profiles better matched the theoretical profiles when they were non-dimensionalised using a wall temperature of 13.4°C rather than T_C = 11.3°C.

Conclusions

Planar temperature and velocity measurements were performed simultaneously using 2-colour/2-dye LIF and PIV of the natural convection flow in a differentially heated cubical cavity at a Rayleigh number of Ra = 3.1 $\times 10^8$. In addition to observing the formation of the boundary layers and intrusion flow, the temperature and velocity profiles in the boundary layers were compared to the theoretical profiles and found to agree well. The local and wall-integrated Nusselt number were estimated and similar to the numerical values after the transient effects had passed.

The results demonstrate the ability of simultaneous 2-colour/2-dye LIF and PIV to quantitatively measure the cold wall thermal and hydrodynamic boundary layers, which are necessary for computing important quantities such as heat transfer and turbulent heat flux. With further development, such experimental measurements could be used to validate numerical simulations of natural convection flows in differentially heated cavities.

Acknowledgements

The financial support of the Australian Research Council (Discovery Project grant DP130100900) is gratefully acknowledged.

References

[1] Armfield, S.W. and Patterson, J.C., Wave properties of natural-convection boundary layers, *J. Fluid Mech.*, **239**, 1992, 195–211.

[2] Estrada-Pérez, C.E., Tan, S. and Hassan, Y.A., Whole-field temperature and velocity measurements for two-phase flow using PIV/LIF, in *ASME/JSME 2011 8th Thermal Engineering Joint Conference*, ASME, 2011, 1–11.

[3] Ostrach, S., An analysis of laminar free-convection flow and heat transfer about a flat plate parallel to the direction of the generating body force, NACA-TN-2635, NACA, 1952, 1–47.

[4] Paolucci, S., The differentially heated cavity, *Sadhana*, **19**, 1994, 619–647.

[5] Sakakibara, J. and Adrian, R.J., Whole field measurement of temperature in water using two-color laser induced fluorescence, *Exp. Fluids*, **26**, 1999, 7–15.

[6] Schöpf, W. and Patterson, J.C., Natural convection in a side-heated cavity: visualization of the initial flow features, *J. Fluid Mech.*, **295**, 1995, 357–379.

[7] Schöpf, W. and Patterson, J.C., Visualization of natural convection in a side-heated cavity: Transition to the final steady state, *Int. J. Heat Mass Transfer*, **39**, 1996, 3497–3509.

[8] Trias, F.X., Gorobets, A., Soria, M. and Oliva, A., Direct numerical simulation of a differentially heated cavity of aspect ratio 4 with Rayleigh numbers up to 10^{11} - Part I: Numerical methods and time-averaged flow, *Int. J. Heat Mass Transfer*, **53**, 2010, 665–673.

[9] Yen, J., Lei, C. and Patterson, J.C., Modelling turbulent buoyancy-driven flows in a differentially heated cavity with horizontal fins, in *10th Australasian Heat and Mass Transfer Conference*, 2016, 1–6.